HHS Public Access

Author manuscript

Nanomedicine. Author manuscript; available in PMC 2016 May 01.

Published in final edited form as:

Nanomedicine. 2015 May ; 11(4): 959–967. doi:10.1016/j.nano.2015.01.013.

Bioactive Silica Nanoparticles Reverse Age-Associated Bone Loss in Mice

M. Neale Weitzmann[#1,2,3,*], **Shin-Woo Ha**[#2], **Tatyana Vikulina**[2], **Susanne Roser-Page**[1,2], **Jin-Kyu Lee**[4], and **George R. Beck Jr.**[1,2,3,*]

[1] The Atlanta Department of Veterans Affairs Medical Center, Decatur, Georgia 30033, USA

[2] Emory University, Department of Medicine, Division of Endocrinology, Atlanta, Georgia, 30322, USA

[3] The Winship Cancer Institute, Emory University School of Medicine, Atlanta GA 30322, USA

[4] Department of Chemistry, Seoul National University, Seoul 151-747, Korea

[#] These authors contributed equally to this work.

Abstract

We recently reported that *in vitro*, engineered 50 nm spherical silica nanoparticles promote the differentiation and activity of bone building osteoblasts but suppress that of bone-resorbing osteoclasts. Furthermore, these nanoparticles promote bone accretion in young mice *in vivo*. In the present study the capacity of these nanoparticles to reverse bone loss in aged mice, a model of human senile osteoporosis, was investigated. Aged mice received nanoparticles weekly and bone mineral density (BMD), bone structure, and bone turnover was quantified. Our data revealed a significant increase in BMD, bone volume, and biochemical markers of bone formation. Biochemical and histological examinations failed to identify any abnormalities caused by nanoparticle administration. Our studies demonstrate that silica nanoparticles effectively blunt and reverse age-associated bone loss in mice by a mechanism involving promotion of bone formation. The data suggest that osteogenic silica nanoparticles may be a safe and effective therapeutic for counteracting age-associated bone loss.

Keywords

Silica nanoparticles; osteoporosis; bone formation; aging; toxicity

Corresponding Authors: M. Neale Weitzmann, Ph.D., 101 Woodruff Circle, 1305 WMRB, Atlanta, Georgia 30322-0001, Tel: (404) 727-1389, Fax (404) 727-1300, mweitzm@emory.edu and George R. Beck Jr., Ph.D., 101 Woodruff Circle, 1026 WMRB, Atlanta, Georgia 30322-0001, Tel: (404) 727-1340, Fax (404) 727-1300, george.beck@emory.edu.

[*]Drs. Weitzmann and Beck have contributed equally to these studies as senior authors

Conflict of interest: The authors declare no competing financial interests.

Aging is a pivotal risk factor for bone loss that often leads to osteoporosis, a devastating disease of the skeleton.[1] Osteoporosis is now considered a major and growing public health concern with 24 million people projected to have osteoporosis in the US alone, and contributing to more than 1.3 million fractures per year.[2] Vertebral fractures are associated with chronic back pain and deformity while hip fracture management requires surgical intervention and is associated with one-year mortality rates of 24% to 30% in the aged and with up to 75% of survivors requiring rehabilitation in long-term care facilities.[3-5] The annual financial burden of fracture management in the US is projected to reach an alarming $25 billion by 2025.[6]

In adults, bone is remodeled throughout life by the coordinated action of bone resorbing osteoclasts that remove old bone, and by bone-building osteoblasts that secrete and mineralize new bone matrix.[7] Shortly after attainment of peak bone mass in early adulthood osteoclastic bone resorption begins to outpace osteoblastic bone formation leading to progressive bone loss. Although women undergo an additional skeletal assault at the time of the menopause owing to estrogen deprivation, both sexes loose significant amounts of bone mass as they age ultimately resulting in high rates of osteoporosis and increased risk of fractures in aged populations.[8, 9] Therapeutic strategies to limit bone loss and prevent fracture are predominantly centered on the suppression of bone resorbing osteoclasts such as bisphosphonates, the most commonly prescribed anti-resorptive agents. Anti-resorptive drugs act mainly by reducing bone turnover (the balance of bone formation and resorption) thus preserving remaining bone mass, rather than improving skeletal architecture.[10] Although anti-resorptive drugs may lead to modest gains in BMD over time, clinical studies reveal that these agents also potently blunt bone formation[11], a likely consequence of the tightly coupled process of bone formation and bone resorption.[10] Anti-resorptive agents are thus inefficient at regenerating lost bone mass and consequently the discovery and development of anabolic drugs capable of actively promoting osteoblastic bone formation is now an area of intensive investigation.

Nanotechnology has begun to revolutionize medicine and drug development (nanomedicine) with the creation of novel nanomaterials for the targeting, visualization and/or delivery of therapeutic cargo.[12] The silica nanoparticles chosen for this study were designed and synthesized using the Stöber method to be suitable for both *in vivo* therapeutic applications as well as *in vitro* mechanistic investigations.[13, 14] These nanoparticles comprise a silica shell (NP1) with an electron dense cobalt ferrite magnetic core (NP1-MNP) which has been used successfully for intracellular localization studies.[15] The silica shell prevents potential toxicity from the release of cobalt ions from the core as well as supporting the incorporation of the fluorescent dye, rhodamine B (590 nm fluorescent emission), which is chemically bonded into the silica shell, and used for *in vitro* visualization of nanoparticles in cells by microscopy. The choice of silica for the shell further facilitates high dispersibility of the nanoparticles into solutions including alcohols, water, and physiological buffers such as PBS and in a wide range of pHs owing to the absence of amine groups.[13] Finally, silica allows for convenient surface modification including decoration by polyethylene glycol (NP1-MNP-PEG) that increases *in vivo* circulation time and enhances biological performance.

This formulation of nanoparticles has been specifically demonstrated to promote osteoblast differentiation and inhibit osteoclast differentiation *in vitro*.[15-17]

Although dietary silica per se is considered non-toxic and defined as a "generally regarded as safe" (GRAS) material by the US Food and Drug Administration (FDA), (GRAS Notice Inventory: GRN 000321), when materials are reduced from bulk form to the nano size range, it is necessary to reexamine toxicity empirically. Data on silica nanoparticle toxicity is conflicting and in part may be related to size distribution, shape, hydrophilicity, porosity, and the possibility of unrecognized or unexpected negative effects by contaminants such as surfactants, and other factors resulting from the synthesis method.[18] An extensive *in vitro* safety profiling of these osteogenic nanoparticles (NP1, NP1-PEG and NP1-MNP) was recently performed using nineteen different cell lines representing all major organ types. The results revealed little toxicity in any cell type analyzed as well as a favorable *in vitro* therapeutic index for nanoparticle-induced mineralization of osteoblast lineage cells such as primary bone marrow stromal cells (osteoblast precursors) and MC3T3-E1 pre-osteoblasts.[17] The favorable *in vitro* therapeutic index emphasizes the potential therapeutic applications of spherical silica nanoparticles for bone disease.

The present study investigated whether the 50 nm silica based nanoparticle NP1-MNP-PEG may have an application in the treatment or prevention of age-associated osteoporosis using a murine model of senile osteoporosis. The studies revealed that NP1-MNP-PEG effectively blunts and reverses age-associated bone loss in aged mice by a mechanism involving promotion of bone formation and without microscopic or biochemical evidence of organ cytotoxicity.

Methods

Synthesis and characterization of Silica nanoparticles (NP1-MNP-PEG)

The spherical 50 nm fluorescent core-shell silica nanoparticle (NP1-MNP) was synthesized by first synthesizing a magnetic cobalt ferrite nanoparticle (MNP) by co-precipitation method followed by addition of silica shell using the hydrolysis and condensation on the surface of MNP induced by Polyvinyl pyrrolidone (PVP, Mw 55k) with incorporation of the fluorescent dye Rhodamine B. Following purification, the additional reaction of poly-ethylene glycol (PEG) having trialkoxysilane (PEG-Si) on the surface of NP1-MNP was used to produce NP1-MNP-PEG. Details about materials used and procedures for characterization including Transmission Electron Microscopy (TEM) for shape and size distribution as well as changes in zeta potential have been previously reported in detail.[13, 15, 16, 19]

Animal Studies—Animal studies were approved by the Emory University Animal Care and Use Committee. Mice were housed under specific pathogen free conditions and fed gamma-irradiated 5V02 mouse chow (Purina Mills, St. Louis, MO), and autoclaved water ad libitum. The animal facility was kept at 23 ± 1°C, with 50% relative humidity and a 12/12 light/dark cycle.

Nanoparticle administration to mice in vivo

For dose response studies female, 2 month old mice (18-20 grams) were injected intraperitoneal (IP) with NP1-MNP-PEG (3, 10, 30 or 50 mg/Kg) suspended in PBS once per week for 2 months. Aged (20 months of age) female wild type C57BL6 mice (~25-30 grams) were purchased from the National Institute on Aging (NIA) aged mouse colony at Charles River Laboratories (Wilmington, MA) and injected with NP1-MNP-PEG (30 mg/Kg) or vehicle once per week for 4 months. Nanoparticles were diluted from a stock concentration of 5 mg/ml using PBS and 150-180 μl injected IP.

Bone densitometry—BMD (g/cm^2) quantifications were performed in anesthetized mice by dual energy X-ray absorptiometry (DXA) using a PIXImus 2 bone densitometer (GE Medical Systems). Region of interest boxes were placed to quantify the femur as previously described.[20] The left and right femurs were averaged for each mouse and the mean femoral BMD/mouse used for group calculations.

Micro-Computed Tomography—Micro-Computed Tomography (μCT) was performed in the femoral epiphysis of mice *ex vivo* to assess trabecular and cortical bone microarchitecture using a μCT40 scanner (Scanco Medical AG, Bruettisellen, Switzerland) calibrated weekly with a factory-supplied phantom. A total of 55 tomographic slices were taken at the femoral epiphysis and trabecular bone segmented from the cortical shell for a total area of 0.6 mm beginning approximately 0.5 mm from the growth plate at a voxel size of 6 μm (70 kVp and 114 mA, and with 200 ms integration time). Projection images were reconstructed using the auto-contour function for trabecular bone. Cortical bone was quantified at the femoral mid-diaphysis from 100 tomographic slices. Representative samples based on BV/TV were reconstructed in 3D to generate visual representations. Indices and units were standardized per published guidelines.[21]

Biochemical indices of bone turnover—Carboxy-terminal telopeptide of type I collagen (CTx) and osteocalcin (Osc), specific and sensitive biochemical markers of bone resorption and bone formation, respectively, were quantified in mice serum using RATlaps (CTx) and Rat-MID (osteocalcin) enzyme-linked immunosorbent assays (ELISAs) (Immunodiagnostic Systems Inc. Fountain Hills AZ). Assays were performed according to the manufactures protocol.

Toxicological studies

At the completion of the study the mice were euthanized and serum and organs collected (Liver, Kidney, Spleen, and Brain) and fixed in 10% Neutral Buffered Formalin (NBF) for histology. The serum was analyzed by ELISA for creatinine, a marker of kidney function, and TNFα, a marker of systemic inflammation, using ELISAs from R & D Systems (Minneapolis, MN). Liver function was assessed by Alanine aminotransferase (ALT) using an ELISA from Abcam (Cambridge, MA). Fixed tissues were paraffin embedded and sections stained with Hematoxylin and Eosin (H&E) for microscopic analysis.

Cell Culture mineralization studies—Human Embryonic Kidney cells (HEK) were cultured in Dulbecco's Modification of Eagle's Medium (Cellgro, Corning, Manassas, VA)

supplemented with 10% fetal bovine serum (FBS; Atlanta Biologicals, Lawrenceville, GA). Human Aortic Smooth Muscle cells were cultured in Medium 231 supplemented with 10% Smooth Muscle Growth Supplement (Gibco, Life technologies, Grand Island, NY) and kindly provided by Dr. Alejandra San Martín (Emory University, Atlanta, GA.,USA). All cell lines were cultured at 37 °C in 5% CO_2. For mineralization studies, cells were plated in osteoblast differentiation medium; α-Modified Eagle's Medium (Thermo Scientific, Waltham, MA) supplemented with 10% FBS, 10 mM β-glycerophosphate and 50 μg/ml ascorbic acid (Sigma-Aldrich, St. Louis, MO) with medium change twice weekly as described previously.[22] Mineralization was visualized by staining with 40 mM Alizarin red S (Sigma) for 15 min. Excess stain was removed by washing with distilled water more than 3 times.

RNA isolation, cDNA synthesis, and quantitative real-time PCR—RNA was extracted using TRIzol reagent (Invitrogen) and cDNA synthesized using QuantiTech Reverse Transcription kit (Qiagen, Valencia CA). qRT-PCR was performed using VeriQuest SYBR Green qPCR master mix (Affymetrix, Santa Clara CA) on a StepOnePlus thermocycler (Applied Biosystems, NY). Primers were designed using qPrimerDepot software (http://primerdepot.nci.nih.gov) and synthesized by Integrated DNA Technologies, Inc. (Coralville, IA) with sequences as follows; 18S (control): F-5'-CAGCCACCCGAGATTGAGCA-3', R-5'-TAGTAGCGACGGGCGGCGTG-3'. ALP: F-5'-CTATCCTGGCTCCGTGCTC-3', R-5'-GCTGGCAGTGGTCAGATGTT-3'. OSC: F-5'-TGAGAGCCCTCACACTCCTC-3', R-5'-CCTCCTGCTTGGACACAAAG-3'. Runx2: F-5'-CAGTAGATGGACCTCGGGAA-3', R-5'-CCTAAATCACTGAGGCGGTC-3'. Fold change was calculated using the $2^{-\Delta\Delta CT}$ method.[23]

Statistical Analyses—Statistical significance was determined using GraphPad InStat version 3 for Windows XP (GraphPad Software, La Jolla, CA). Simple comparisons were made with unpaired Student's t test for parametric data or Mann-Whitney for non-parametric data. Welch's correction was applied to any data with significant variances determined by F test. Multiple comparisons were performed by repeated measures ANOVA with Bonferroni multiple comparisons *post* test. (*) $p<0.05$ was considered significant. One significant outlier (determined by Grubbs' test, using an alpha of 0.05) in the osteocalcin vehicle group (Figure 1, *D*) falling 3 SD from the mean was excluded from analysis.

Results

NP1-MNP-PEG reverses age-associated bone loss in mice

Age-associated bone loss is a significant cause of osteoporosis in both men and women. Like humans, mice undergo a significant decline in BMD and bone mass as they age. The average lifespan of a laboratory mouse is about 2 years (depending on strain) and 18-24 months of age is considered old in a mouse where 50% survivorship is around 28 months. Thus mice 24 months of age (the endpoint of our study) corresponds roughly to a human of 69 years of age.[24] To assess the potential for osteogenic NP1-MNP-PEG silica nanoparticles to alleviate bone loss associated with aging, old (20 months old) female C57BL6 mice were

injected once per week intraperitoneal for 16 weeks with vehicle (PBS) as a control, or NP1-MNP-PEG (30 mg/Kg/week). Femoral BMD was quantified prospectively by DXA at monthly intervals for 4 months (up to 24 months of age). Results revealed that while vehicle injected mice continue to undergo age-associated loss of BMD at the femur, NP1-MNP-PEG administration stalled bone loss after just 2 months of treatment and significantly ($p<0.05$) reversed bone loss by 16 weeks of treatment (Figure 1, *A*).

NP1-MNP-PEG preferentially increases trabecular relative to cortical bone

Cortical bone represents approximately 80% of bone mass and is the outer hard shell of bone characterized by slow turnover, whereas trabecular (cancellous or spongy) bone is more metabolically active and subject to higher turnover.[25] Whereas DXA provides an integrated areal (2 dimensional) extrapolation of cortical and trabecular BMD over relatively large areas (entire femurs) prospectively over time, μCT is capable of generating high resolution volumetric (3 dimensional) trabecular BMD (TV.D.) and independent cortical and trabecular architectural indices of bone structure. To provide independent evaluations of the two major bone compartments (cortical and trabecular) μCT was performed on isolated femurs *ex vivo* after 4 months of treatment. Two representative high resolution (6 μm) μCT reconstructions (labeled 1 and 2) of trabecular bone (Figure 1, *B*, left panel) and cortical bone (Figure 1, *B*, right panel) from vehicle and NP1-MNP-PEG treated aged mice revealed increases in trabecular, but not cortical, bone.

Quantitative microarchitectural indices of trabecular bone structure were further computed for vehicle and NP1-MNP-PEG treated mice (Table 1). Femoral trabecular bone volume fraction, the key index of trabecular bone mass (Bone volume/Total volume - BV/TV) was significantly increased in aged mice receiving NP1-MNP-PEG as a consequence of both a significant increase in overall trabecular bone volume (BV) as well as a contribution from a smaller, but significant, increase in total tissue volume (TV) relative to control. This increase in BV/TV was consistent with a 42% increase in trabecular density (TV.D.), a 15% decline in trabecular separation (Tb. Sp.), reflecting the distance between trabecular elements and a 21.5% increase in trabecular number (Tb. N.), the number of rod like structures forming the trabecular compartment (Table 1), Although these structural indices each showed a strong trend they did not reach statistical significance. The likely reason for this is that trabecular bone is rapidly depleted in the femurs during mice aging, leading to a relatively high population standard deviation that makes it difficult to achieve statistical significance in the structural indices, without resorting to impractical numbers of animals. Cortical bone was quantified in the mid-femoral diaphysis and consistent with visual cues (Figure 1, *B*) revealed no significant increase in cortical thickness (Co. Th.) or Cortical volume (Co. Vol.), two important indices of cortical mass. Taken together, the μCT data suggest that the increase in bone mass promoted by NP1-MNP-PEG nanoparticles was likely associated with increases in the trabecular compartment and that the increase in BV/TV was predominantly associated with an increase in the number of new trabecular rods formed.

NP1-MNP-PEG enhances biochemical indices of bone formation but not indices of bone resorption in vivo

Increases in bone mass may be explained by changes in bone formation, bone resorption, or both. To assess the rates of bone resorption and bone formation *in vivo* biochemical bone turnover markers were quantified in the serum of vehicle and NP1-MNP-PEG treated mice. Serum CTx is a sensitive and specific marker of *in vivo* bone resorption and was not significantly changed between vehicle and NP1-MNP-PEG treated groups (Figure 1, *C*). By contrast, serum osteocalcin, a sensitive and specific biochemical marker of *in vivo* bone formation was increased by 3 fold in NP1-MNP-PEG treated mice (Figure 1, *D*). These data suggest that the increase in BMD was a likely consequence of elevated bone formation.

NP1-MNP-PEG dose dependently increases BMD in mice

In order to determine the dose dependency of NP1-MNP-PEG *in vivo* we examined bone accretion in female C57BL6 mice (2 months of age) injected IP weekly for 8 weeks with vehicle (PBS) as a control or NP1-MNP-PEG (3, 10, 30 or 50 mg/Kg/week). Femoral BMD was quantified by DXA at 2 months of treatment. Dose responsive increases in BMD were observed between 10 and 50 mg/kg (Figure 2).

NP1-MNP-PEG does not result in obvious organ damage in aged mice

Organ damage is a significant concern for the development of any new pharmaceutical agent, therefore liver and kidney toxicity were examined (two organs mainly involved in drug and nanoparticle clearance *in vivo*) by quantifying serum markers of liver and kidney damage/toxicity using ALT and creatinine, respectively. No significant changes were observed for either marker of organ function (Table 2). We additionally performed gross histological examinations of potential target organs including liver, kidney, spleen, and brain by H&E staining (Figure 3 *A,B*). No gross abnormalities were observed in any tissue analyzed including brain even though NP1-MNP has been previously suggested to penetrate the blood-brain barrier.[26]

To determine if injection of the nanoparticles initiated an inflammatory response TNFα was measured in serum and no significant change was found between the groups (Table 2). Collectively, the data suggest that 50 nm silica nanoparticles have biological activity that prevents bone loss in aging mice by promoting bone formation, without gross microscopic or biochemical evidence of organ damage.

NP1-MNP-PEG does not result in calcification of non-mineralizing cells

To determine if the mineralization promoting effects of silica nanoparticles are specific to osteoblasts or if they could induce trans-differentiation, the ability take on the characteristics of a different cell type, leading to ectopic vascular or kidney calcifications, human aortic smooth muscle cells (HASMCs) and human embryonic kidney cells (HEKs) were treated every 2 to 3 days with nanoparticles. Osteoblast differentiation medium (AA+βGP) and inorganic phosphate (2 mM) was used as a positive control to promote calcium deposition. Following 11 days of treatment cells were either stained with Alizarin red S (calcium deposition) or parallel plates harvested for osteoblastic gene analysis by real time RT-PCR

quantification of mRNA. The results revealed that silica nanoparticle treatment had no effect on calcium deposition at concentrations up to 50 μg/ml (Figure 4 *A,B*; top panels) in either aorta or kidney cells. This concentration is well beyond the effective concentration 50 (EC_{50}) for osteoblastic cells (previously defined as 17.8 μg/ml) and the EC_{90} (47.8 μg/ml).[17] Analysis of key osteoblast differentiation marker genes by qRT-PCR found no stimulatory effects in response to increasing concentration of silica nanoparticles in either cell type (Figure 4 *A,B*; bottom panels) whereas osteoblasts respond robustly to the nanoparticles with increased gene expression.[15-17] Taken together with previous studies, the results suggest that 50 nm silica nanoparticles very effectively and selectively induce mineralization and differentiation of the osteoblast lineage cells without a detectable effect on vascular or kidney cell types.

Discussion

Previous reports have shown that 50 nm engineered silica nanoparticles are capable of promoting accretion of bone mass in young mice (2-4 months of age). Mice achieve peak bone mass at approximately 4-6 months, although this may vary by strain.[27] Therefore, this previous study examined mice undergoing bone modeling, a stage at which the rates of bone formation and bone resorption are both high and osteoclasts and osteoblasts are highly responsive to external stimuli.[16] Upon achieving peak bone mass there is a slow but steady decline in skeletal mass and architecture which continues progressively throughout the remaining life span of the laboratory mouse.[28] This bone loss is considered similar to what occurs in human aging[29] making the mouse a valuable model for the study of age-related bone loss (senile osteoporosis). Further, the use of the aged mouse model examines the process of bone remodeling as opposed to the bone modeling that occurs in younger mice (representative of bone accretion in human children). In this model silica nanoparticles (NP1-MNP-PEG) were effective in not only stalling age-related bone loss, but led to a significant increase in BMD and volume, suggesting a capacity to regenerate lost trabecular bone mass.

It was previously reported that silica nanoparticles both stimulate osteoblast differentiation and mineralization and suppress osteoclast differentiation *in vitro*.[16] However whether bone accretion *in vivo* was a consequence of increased bone formation, diminished bone resorption or a combination of both remained unclear because nanoparticles were administered acutely and then discontinued. This resulted in the biochemical markers, which are transient, to return to baseline by the end of the study. Interestingly, our data now demonstrate that the nanoparticle-induced increase in BMD and bone volume *in vivo* are predominantly a consequence of an increase in bone formation (quantified by *in vivo* bone turnover markers) rather than a decrease in bone resorption or by a combination of mechanisms. This is an important outcome with high clinical significance, as currently there are numerous anti-resorptive drugs available for the prevention of bone loss in osteoporotic conditions, but only one FDA approved anabolic agent (Teriparatide, a fragment of human parathyroid hormone) capable of promoting bone formation.[10] The necessity of frequent (daily) injection and the high cost of this biologic have reduced its impact and there is consequently a need for the development of new anabolic agents for the treatment of osteoporosis.

The reasons for the difference between *in vivo* and *in vitro* remains unclear, however it is possible that the unique effect on bone formation (osteoblast activity) is due to cell or tissue localization or differences in effective dose between *in vitro* and *in vivo* studies. One possible explanation for the unique osteoblastic activity of these nanoparticles is that mechanistically, NP1 and its derivatives function in part, by antagonizing the activation of the NF-κB signal transduction pathway, suppressing osteoclast differentiation but simultaneously stimulating osteoblast differentiation and mineralization.[16] Bone formation in mice *in vivo* is extremely sensitive to NF-κB activation, more so than osteoclastogenesis, as demonstrated by the fact that *in vivo* ablation of TNFα, a potent inducer of NF-κB and inhibitor of osteoblasts, leads to a significant increase in bone formation without any effects on osteoclastic bone resorption.[30] It is thus possible that the two cell types are exposed to lower concentrations of nanoparticles *in vivo* relative to *in vitro* resulting in preferential effects on the more sensitive osteoblasts. Higher doses of nanoparticles thus may facilitate activation of both pathways intensifying the observed effects.

How nanoparticles reach the sites of bone turnover is not completely elucidated. However, as the peritoneal cavity is highly vascularized the nanoparticles are likely absorbed through the vasculature and carried though the peripheral circulation to bone and bone marrow, which too is highly vascularized. We have previously demonstrated the high affinity of silica nanoparticles for collagen[19] which is the predominant protein in bone and consequently there is a potential for retention of nanoparticle in the bone microenvironment through association with bone collagen. Further, these nanoparticles are known to be retained in cultured osteoblasts for weeks after a single exposure even passing the nanoparticles to daughter cells upon division.[19] Like most nanomaterials, scavenging macrophages, the kidney, and reticuloendothelial system of the liver are likely responsible for processing and excretion of the bulk of the circulating nanoparticles not retained in the skeleton or other tissues. The PEGylation of the surface of the nanoparticles however, has been demonstrated to increase circulation time in part by avoidance of the reticuloendothelial system, and thus increasing the potential for nanoparticle internalization by osteoblasts and their precursors.

In addition to functional mineralization some cell types such as vascular smooth muscle and kidney in pathological states can be susceptible to calcification and in the case of smooth muscle cells it is hypothesized that a trans-differentiation occurs in that the smooth muscle cells leading to an osteoblast phenotype and expression of osteoblast markers genes such as Runx2 and osteocalcin.[31] Previous studies on 50 nm silica nanoparticles have revealed that although the two cells most closely associated with bone metabolism, osteoblasts and osteoclasts precursors, readily take up the nanoparticles within hours of exposure, many other cells types if exposed for long enough periods of time, up to 72 hours, will also take up the nanoparticles.[17, 19] Studies presented herein suggest that chronic exposure to the 50 nm silica nanoparticles does not directly enhance calcification of vascular smooth muscle or kidney cells. Further, gene expression studies suggest that the nanoparticles do not induce an osteoblastic phenotype in non-osteoblastic cells. Taken together the results suggest that the ability of the silica nanoparticles to enhance osteoblast mineralization is mostly targeted to

the osteoblast lineage although the underlying mechanism(s) for the specificity remain to be fully elucidated.

Although there is still much to be elucidated about the mechanisms underlying aging, the process is generally thought to include damage to cell function resulting in systemic changes which ultimately alters the way the body responds to both internal and environmental stimuli.[32] Aging is therefore not only a risk factor for bone loss,[1] but also for immunosenescence, a progressive decline in responsiveness to exogenous antigens and a paradoxical increase in autoimmunity leading to a chronic inflammatory state that has been referred to as "inflammaging".[33] Aging is also suggested to negatively impact certain pharmacological parameters including the kinetics of bioavailability, tissue distribution, and hepatic drug clearance and possibly the glomerular filtration rate of the kidney.(review in[34]) Although silica based nanomaterials are generally considered relatively non-toxic, aging is a factor which has been minimally addressed to date. Most studies attempting to define the negative and positive effects of nanomaterials on cells and tissue have been performed for hours, days, or in a small number of cases weeks, and almost exclusively in younger rodents (8+ weeks) (reviewed in[35, 36]). To our knowledge this is one of the first studies to evaluate the effects of a nanomaterial in aged mice. The mice in the present study, generally representing a 69 year old human, were treated for four months providing insights into the effects of silica nanoparticles on both long-term exposure as well as the effects in the elderly. The results identified no negative impact of long-term silica nanoparticle exposure or age on the general toxicology endpoints tested while positively impacting bone.

In summary, the data presented herein suggest a potential for silica based nanoparticles to be further developed for their intrinsic bone enhancing properties. Collectively, the studies suggest that 50 nm silica nanoparticles may be an effective therapeutic agent for counteracting bone loss in pathological conditions including age-associated osteoporosis with limited off-target effects.

Acknowledgments

Funding: This study was supported in part by grants from NIAMS (AR056090), the Georgia Research Alliance (GRA.VL12.C2) and the Center for Pediatric Nanomedicine (RC159-G3) sponsored by Emory University, the Department of Biomedical Engineering at Georgia Institute of Technology, and Children's Healthcare of Atlanta, Atlanta, GA, USA to M.N. Weitzmann and G.R. Beck Jr. M.N. Weitzmann is also supported in part by funding from the Biomedical Laboratory Research & Development Service of the VA Office of Research and Development (5I01BX000105) and by grants AR059364 and AR053607 from NIAMS and AG040013 from NIA. G.R. Beck Jr. is also supported by a Biomedical Laboratory Research & Development Service Award Number I01BX002363 from the VA Office of Research and Development and in part by a grant from the NCI (CA136716). The content of this manuscript is solely the responsibility of the authors and does not represent the official views of the Department of Veterans Affairs, the National Institutes of Health, or the United States Government.

References

1. Streckfus CF, Parsell DE, Streckfus JE, Pennington W, Johnson RB. Relationship between oral alveolar bone loss and aging among African-American and Caucasian individuals. Gerontology. 1999; 45:110–4. [PubMed: 9933734]
2. Kanis JA. Assessment of fracture risk and its application to screening for postmenopausal osteoporosis: synopsis of a WHO report. WHO Study Group. Osteoporos Int. 1994; 4:368–81. [PubMed: 7696835]

3. Kates SL, Kates OS, Mendelson DA. Advances in the medical management of osteoporosis. Injury. 2007; 38(Suppl 3):S17–23. [PubMed: 17723788]
4. Johnell O, Kanis JA. An estimate of the worldwide prevalence and disability associated with osteoporotic fractures. Osteoporos Int. 2006; 17:1726–33. [PubMed: 16983459]
5. Bass E, French DD, Bradham DD, Rubenstein LZ. Risk-adjusted mortality rates of elderly veterans with hip fractures. Ann Epidemiol. 2007; 17:514–9. [PubMed: 17420142]
6. Burge R, Dawson-Hughes B, Solomon DH, Wong JB, King A, Tosteson A. Incidence and economic burden of osteoporosis-related fractures in the United States, 2005-2025. J Bone Miner Res. 2007; 22:465–75. [PubMed: 17144789]
7. Manolagas SC, Bellido T, Jilka RL. New insights into the cellular, biochemical, and molecular basis of postmenopausal and senile osteoporosis: roles of IL-6 and gp130. Int J Immunopharmacol. 1995; 17:109–16. [PubMed: 7657404]
8. Manolagas SC. From estrogen-centric to aging and oxidative stress: a revised perspective of the pathogenesis of osteoporosis. Endocr Rev. 2010; 31:266–300. [PubMed: 20051526]
9. Almeida M, Han L, Martin-Millan M, Plotkin LI, Stewart SA, Roberson PK, et al. Skeletal involution by age-associated oxidative stress and its acceleration by loss of sex steroids. J Biol Chem. 2007; 282:27285–97. [PubMed: 17623659]
10. Hodsman AB, Bauer DC, Dempster DW, Dian L, Hanley DA, Harris ST, et al. Parathyroid hormone and teriparatide for the treatment of osteoporosis: a review of the evidence and suggested guidelines for its use. Endocr Rev. 2005; 26:688–703. [PubMed: 15769903]
11. Cummings SR, San Martin J, McClung MR, Siris ES, Eastell R, Reid IR, et al. Denosumab for prevention of fractures in postmenopausal women with osteoporosis. N Engl J Med. 2009; 361:756–65. [PubMed: 19671655]
12. Sahoo SK, Parveen S, Panda JJ. The present and future of nanotechnology in human health care. Nanomedicine. 2007; 3:20–31. [PubMed: 17379166]
13. Ha SW, Camalier CE, Beck GR Jr. Lee J-K. New method to prepare very stable and biocompatible fluorescent silica nanoparticles. Chem Commun (Camb). 2009:2881–3. [PubMed: 19436897]
14. Yoon TJ, Yu KY, Kim E, Kim JS, Kim BG, Yun S- H, et al. Specific Targeting, Cell Sorting, and Bioimaging with Smart Magnetic Silica Core-Shell Nanomaterials. Small. 2006; 2:209–215. [PubMed: 17193022]
15. Ha SW, Weitzmann MN, Beck GR Jr. Bioactive silica nanoparticles promote osteoblast differentiation through stimulation of autophagy and direct association with LC3 and p62. ACS Nano. 2014; 8:5898–910. [PubMed: 24806912]
16. Beck GR Jr. Ha SW, Camalier CE, Yamaguchi M, Li Y, Lee JK, et al. Bioactive silica-based nanoparticles stimulate bone-forming osteoblasts, suppress bone-resorbing osteoclasts, and enhance bone mineral density in vivo. Nanomedicine. 2012; 8:793–803. [PubMed: 22100753]
17. Ha SW, Sikorski JA, Weitzmann MN, Beck GR Jr. Bio-active engineered 50nm silica nanoparticles with bone anabolic activity: Therapeutic index, effective concentration, and cytotoxicity profile in vitro. Toxicol In Vitro. 2014; 28:354–64. [PubMed: 24333519]
18. Napierska D, Thomassen LC, Rabolli V, Lison D, Gonzalez L, Kirsch-Volders M, et al. Size-dependent cytotoxicity of monodisperse silica nanoparticles in human endothelial cells. Small. 2009; 5:846–53. [PubMed: 19288475]
19. Ha SW, Camalier CE, Weitzmann MN, Beck GR Jr. Lee JK. Long-term monitoring of the physicochemical properties of silica-based nanoparticles on the rate of endocytosis and exocytosis and consequences of cell division. Soft Materials. 2013; 11:195–203. [PubMed: 24058289]
20. Toraldo G, Roggia C, Qian WP, Pacifici R, Weitzmann MN. IL-7 induces bone loss in vivo by induction of receptor activator of nuclear factor kappa B ligand and tumor necrosis factor alpha from T cells. Proc Natl Acad Sci U S A. 2003; 100:125–30. [PubMed: 12490655]
21. Bouxsein ML, Boyd SK, Christiansen BA, Guldberg RE, Jepsen KJ, Muller R. Guidelines for assessment of bone microstructure in rodents using micro-computed tomography. J Bone Miner Res. 2010; 25:1468–86. [PubMed: 20533309]
22. Beck GR Jr. Sullivan EC, Moran E, Zerler B. Relationship between alkaline phosphatase levels, osteopontin expression, and mineralization in differentiating MC3T3-E1 osteoblasts. J Cell Biochem. 1998; 68:269–80. [PubMed: 9443082]

23. Livak KJ, Schmittgen TD. Analysis of relative gene expression data using real-time quantitative PCR and the 2(-Delta Delta C(T)) Method. Methods. 2001; 25:402–8. [PubMed: 11846609]
24. Flurkey, K.; Currer, JM.; Harrison, DE. The Mouse in Aging Research.. In: Fox, JG.; Barthold, S.; Davisson, M.; Newcomer, CE.; Quimby, FW.; Smith, A., editors. The Mouse in Biomedical Research. Elsevier; 2007. p. 637-672.
25. Seeman E, Delmas PD. Bone quality--the material and structural basis of bone strength and fragility. N Engl J Med. 2006; 354:2250–61. [PubMed: 16723616]
26. Kim JS, Yoon TJ, Yu KN, Kim BG, Park SJ, Kim HW, et al. Toxicity and tissue distribution of magnetic nanoparticles in mice. Toxicol Sci. 2006; 89:338–47. [PubMed: 16237191]
27. Beamer WG, Donahue LR, Rosen CJ, Baylink DJ. Genetic variability in adult bone density among inbred strains of mice. Bone. 1996; 18:397–403. [PubMed: 8739896]
28. Sundberg JP, Berndt A, Sundberg BA, Silva KA, Kennedy V, Bronson R, et al. The mouse as a model for understanding chronic diseases of aging: the histopathologic basis of aging in inbred mice. Pathobiol Aging Age Relat Dis. 2011:1.
29. Halloran BP, Ferguson VL, Simske SJ, Burghardt A, Venton LL, Majumdar S. Changes in bone structure and mass with advancing age in the male C57BL/6J mouse. J Bone Miner Res. 2002; 17:1044–50. [PubMed: 12054159]
30. Li Y, Li A, Strait K, Zhang H, Nanes MS, Weitzmann MN. Endogenous TNFalpha lowers maximum peak bone mass and inhibits osteoblastic Smad activation through NF-kappaB. J Bone Miner Res. 2007; 22:646–55. [PubMed: 17266397]
31. Jono S, McKee MD, Murry CE, Shioi A, Nishizawa Y, Mori K, et al. Phosphate regulation of vascular smooth muscle cell calcification. Circ Res. 2000; 87:E10–7. [PubMed: 11009570]
32. Lopez-Otin C, Blasco MA, Partridge L, Serrano M, Kroemer G. The hallmarks of aging. Cell. 2013; 153:1194–217. [PubMed: 23746838]
33. Salvioli S, Capri M, Valensin S, Tieri P, Monti D, Ottaviani E, et al. Inflamm-aging, cytokines and aging: state of the art, new hypotheses on the role of mitochondria and new perspectives from systems biology. Curr Pharm Des. 2006; 12:3161–71. [PubMed: 16918441]
34. McLean AJ, Le Couteur DG. Aging biology and geriatric clinical pharmacology. Pharmacol Rev. 2004; 56:163–84. [PubMed: 15169926]
35. Lewinski N, Colvin V, Drezek R. Cytotoxicity of nanoparticles. Small. 2008; 4:26–49. [PubMed: 18165959]
36. Magdolenova Z, Collins A, Kumar A, Dhawan A, Stone V, Dusinska M. Mechanisms of genotoxicity. A review of in vitro and in vivo studies with engineered nanoparticles. Nanotoxicology. 2014; 8:233–78. [PubMed: 23379603]

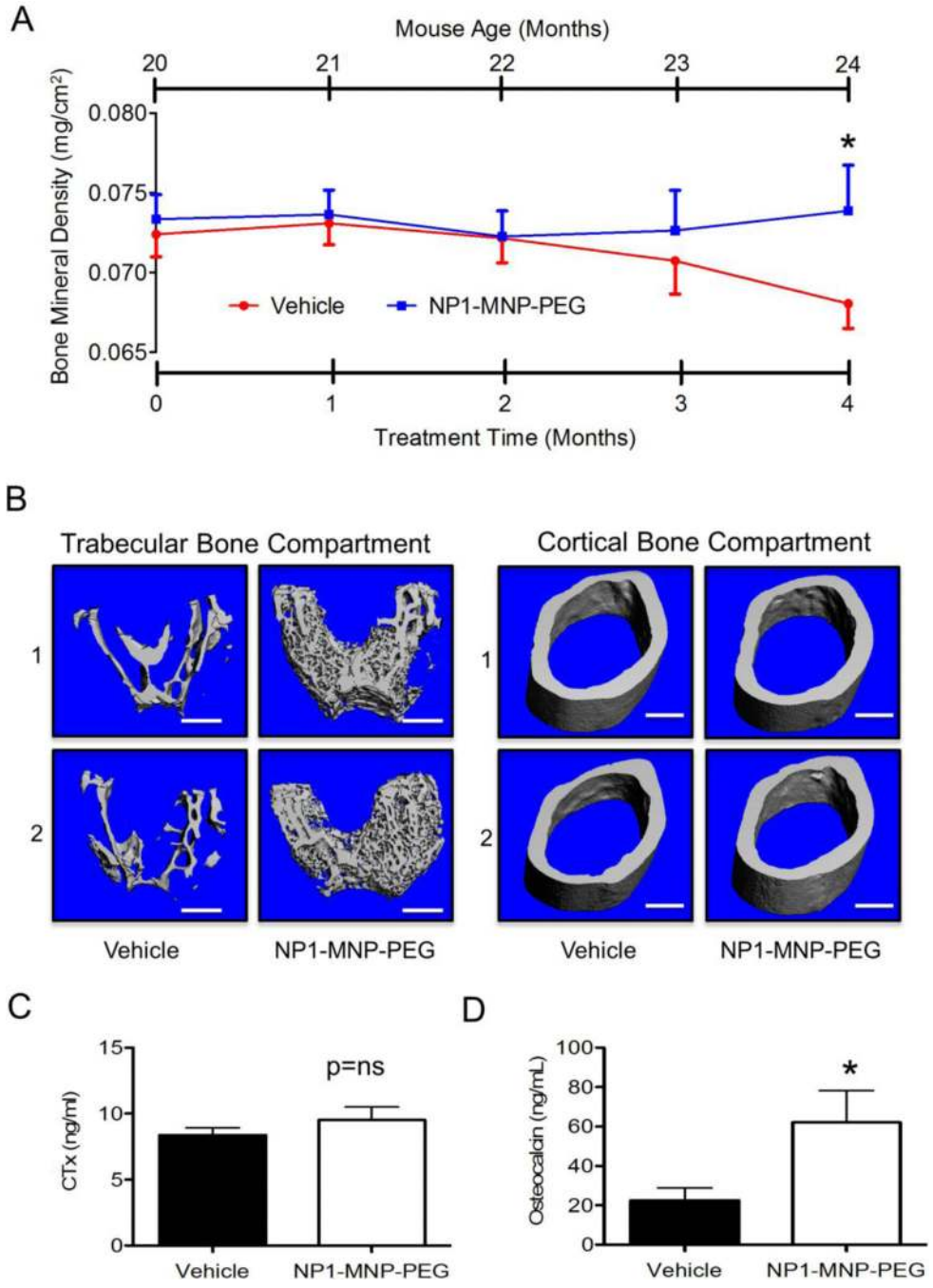

Figure 1. NP1-MNP-PEG stops and reverses age-associated bone loss in aged mice *in vivo*

Aged female C57BL6 mice were injected IP with vehicle (PBS) or 30 mg/Kg/week NP1-MNP-PEG beginning at 20 months of age for 16 weeks. **(A)** Femoral BMD was monitored prospectively by DXA at monthly intervals up to 24 months of age (4 months). *P ≤0.05; N=10-12 mice/group. **(B)** Representative high resolution (6 μm) μCT reconstructions of trabecular (left) and cortical (right) bone compartments from vehicle and NP1-MNP-PEG treated mice. Scale bar (white line) = 500 μm. **(C)** Quantification by ELISA of C-terminal telopeptide of type I collagen (CTx), a marker of *in vivo* bone resorption in vehicle NP1-

MNP-PEG treated mice. **(D)** Quantification by ELISA of serum osteocalcin a marker of *in vivo* bone formation. *P ≤0.05; t-test. N= 8-14 mice/group, ns=not significant.

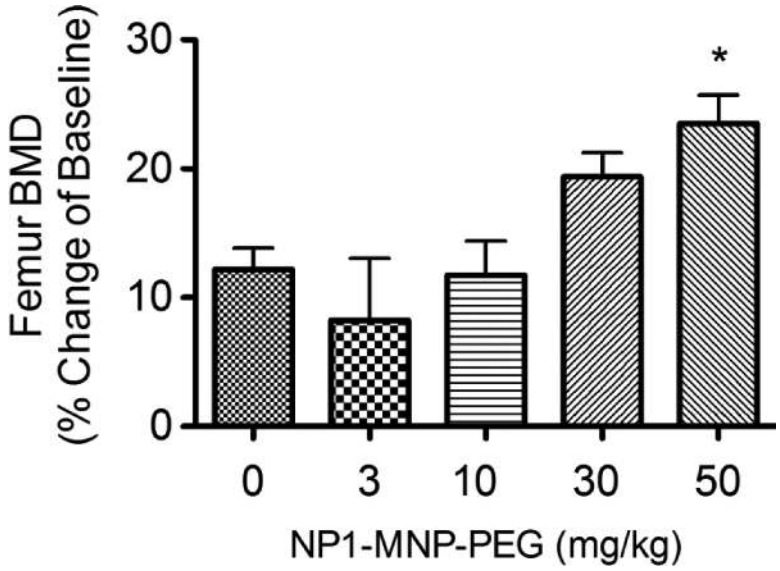

Figure 2. NP1-MNP-PEG dose-dependently increases BMD in young mice

Female C57BL6 mice 8 weeks of age were injected IP with vehicle (PBS) as a control or NP1-MNP-PEG (3, 10, 30 or 50 mg/Kg/week) for 8 weeks and the BMD of the femurs analyzed by DXA. Data presented as percentage change of starting baseline for each mouse (Mean ± SD). *P < 0.05 relative to 0 mg/kg; 1 way ANOVA. N= 9-12 mice/group.

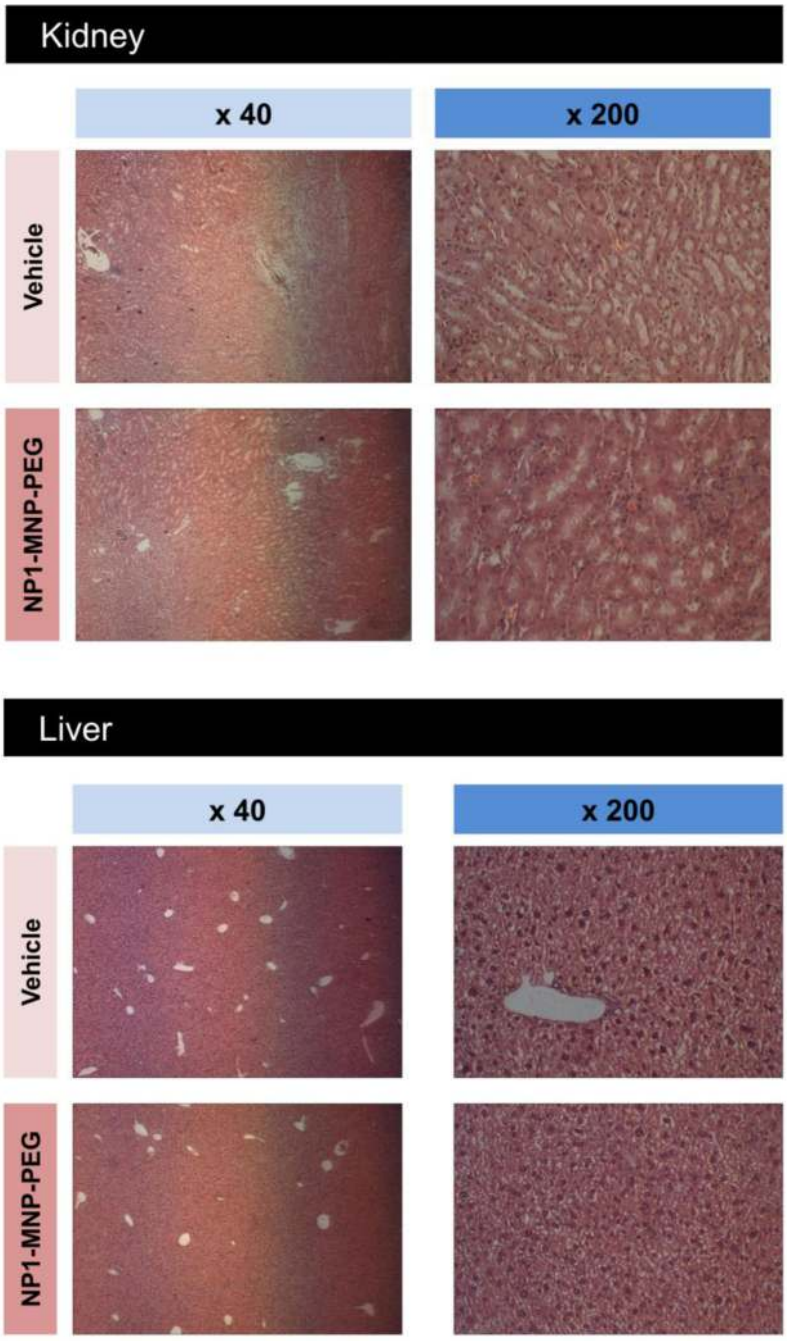

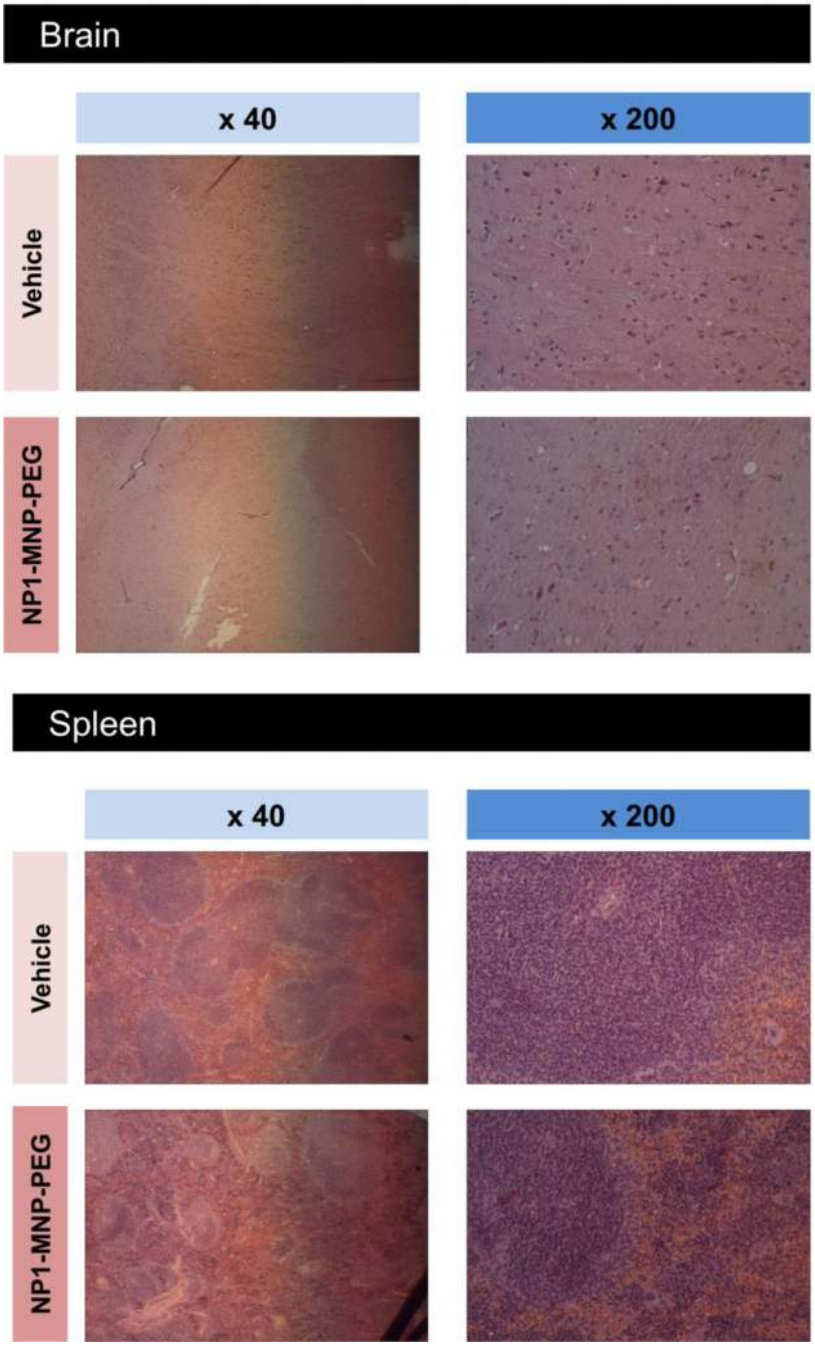

Figure 3. Gross histological analysis of target tissue in aged mice after 4 months of NP1-MNP-PEG treatment

Major organs from aged female C57BL6 mice injected intraperitoneal with vehicle (PBS) or 30 mg/Kg/week NP1-MNP-PEG were collected at the completion of the study including; **(A)** kidney, liver, **(B)** spleen, and brain. Tissues were fixed, sectioned, and stained with H&E and photographed under light microscopy at 40x and 200x magnifications, as indicated.

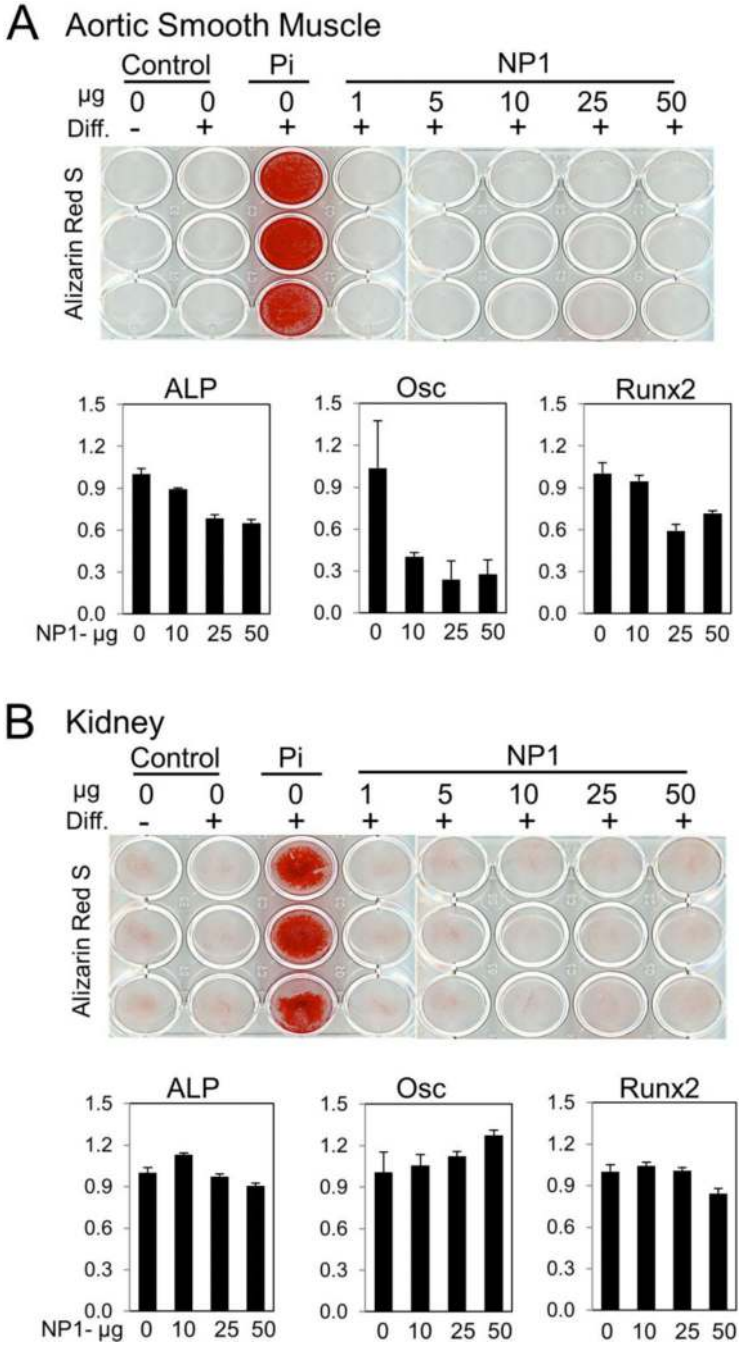

Figure 4. Silica nanoparticles do not induce calcification of non-mineralizing tissues

Human aortic smooth muscle cells **(A)** or human embryonic kidney (HEK) cells **(B)** were cultured in growth medium or osteoblast differentiation medium (Diff.) for 11 days. NP1 was added at the indicated concentrations. Inorganic phosphate (Pi) (2 mM) was used as a positive control. Cells were stained for calcification after 11 days with Alizarin red S. Parallel cultures were harvested for gene expression analyses by qRT-PCR as indicated

(ALP: alkaline phosphatase, Osc: osteocalcin). Results were calculated using the $2^{-\Delta\Delta CT}$ method normalized to 18S, and are expressed as fold change ± SD.

Table 1

Femoral Structural Indices in Aged Mice Treated with NP1-MNP-PEG

Trabecular Indices	Vehicle	NP1-MNP-PEG	% Change	P
TV [mm^3]:	0.7833 ± 0.0555	0.8576 ± 0.0676	+9.5	*0.0164
BV [mm^3] :	0.1137 ± 0.0314	0.1897 ± 0.0927	+66.8	*0.0400
BV/TV [%] :	14.5 ± 3.9	22.1 ± 11.0	+52.0	*0.0482
Tb.Th [mm] :	0.0669 ± 0.0115	0.0627 ± 0.0085	−6.3	0.3975
Tb.N [1/mm]:	7.79 ± 1.10	9.47 ± 3.15	+21.5	0.2286
Tb. Sp [mm]:	0.1913 ± 0.0179	0.1627 ± 0.0512	−15.0	0.1830
TV. D [mg HA/cm^3]:	177.3 ± 50.8	252.1 ± 111.7	+42.2	0.0946
Cortical Indices				
Ct. Ar [mm^3]:	0.4534 ± 0.0216	0.4635 ± 0.0456	2.2	0.5481
Ct. Th [mm]:	1.51 ± 0.08	1.51 ± 0.08	0.0	0.9989

Structural indices: total volume (TV, volume of the entire region of interest), trabecular bone volume (BV, volume of the region segmented as trabecular bone), bone volume fraction (BV/TV), trabecular thickness (Tb. Th; mean thickness of trabeculae, assessed using direct 3D methods), trabecular separation (Tb. Sp; mean distance between trabeculae, assessed using direct 3D methods), trabecular number (Tb. N; Measure of the average number of trabeculae per unit length); and the cortical indices cortical area (Ct. Ar; Cortical bone area = cortical volume (Ct.V) ÷ (number of slices × slice thickness)) and cortical thickness (Ct. Th; average cortical thickness).[21] N=9-11 mice/group

*p<0.05. Mann Whitney.

Table 2

Markers of liver and kidney toxicology and systemic inflammation in aged mice treated for 4 months with vehicle or NP1-MNP-PEG.

Serum Marker	Organ System	Vehicle	NP1-MNP-PEG	P
Creatinine [nmol]	Kidney	5.8 ± 0.7	5.2 ± 1.4	ns
ALT [nmol]	Liver	0.1 ± 0.2	0.07 ± 0.1	ns
TNFα [pg/mL]	Inflammation	13.3 ± 0.8	15.8 ± 2.9	ns

Alanine aminotransferase (ALT). N=9-11 mice/group ± SEM, P= not significant (ns).